C. R. Palevol 9 (2010) 411–422

Contents lists available at ScienceDirect

Comptes Rendus Palevol

www.sciencedirect.com

General palaeontology

Two applications of 3D semi-landmark morphometrics implying different template designs: the theropod pelvis and the shrew skull

Deux applications de morphométrie par semi-landmarks 3D impliquant une conception différente du template : le pelvis des théropodes et le crâne des musaraignes

Thibaud Souter[a,b,*,c,d], Raphael Cornette[b,d], Julio Pedraza[b,d], John Hutchinson[e], Michel Baylac[b,d]

[a] *UMR 7207–CR2P, laboratoire de paléontologie, département histoire de la Terre, centre de recherche sur la paléobiodiversité et les paléoenvironnements, CNRS, Muséum national d'histoire naturelle, 8, rue Buffon, 75005 Paris, France*
[b] *UMR 7205, département systématique et évolution, origine, structure et évolution de la biodiversité (OSEB), CNRS, Muséum national d'histoire naturelle, plateforme morphométrie, bâtiment d'entomologie, 45, rue Buffon, 75005 Paris, France*
[c] *UMR 7179–mécanismes adaptatifs : des organismes aux communautés, département écologie et gestion de la biodiversité, CNRS, Muséum national d'histoire naturelle, pavillon d'anatomie comparée, 55, rue Buffon, 75005 Paris, France*
[d] *UMS 2700–outils et méthodes de la systématique intégrative, plateforme morphométrie, département systématique et évolution, CNRS, Muséum national d'histoire naturelle, bâtiment d'entomologie, 45, rue Buffon, 75005 Paris, France*
[e] *Structure & Motion Laboratory, Department of Veterinary Basic Sciences, The Royal Veterinary College, University of London, Hawkshead Lane, London, Herts AL9 7TA, United Kingdom*

ARTICLE INFO

Article history:
Received 18 March 2010
Accepted after revision 1st September 2010
Available online 16 October 2010

Written on invitation of the Editorial Board

Keywords:
Geometric morphometrics
Semi-landmark
Template
3D
Visualisation
Theropod
Shrew

ABSTRACT

Geometric morphometrics involves defining landmark points to generate a discrete representation of an object. This crucial step is strongly influenced by the biological question guiding the analysis, and even more when using curve and surface semi-landmarks methods, because these require to generate a template of reference. We exemplify these constraints using two datasets from projects with very different backgrounds. The Theropod Dataset is a functional morphometric analysis of different extinct and extant theropod pelves. The Shrew Dataset is a populational morphometric analysis of the white-toothed shrew with very small variations in skull shape. We propose a novel procedure to generate a regular template configuration, using polygonal modelling tools. This method allows us to control the template geometry and adapt its complexity to the morphological variation in the sample. More studies are necessary to assess the morphometric and statistical importance of template design in curve and surface analyses.

© 2010 Académie des sciences. Published by Elsevier Masson SAS. All rights reserved.

* Corresponding author.
E-mail address: souter@mnhn.fr (T. Souter).

1631-0683/$ – see front matter © 2010 Académie des sciences. Published by Elsevier Masson SAS. All rights reserved.
doi:10.1016/j.crpv.2010.09.002

Mots clés :
Morphométrie géométrique
Semi-landmark
Template
3D
Visualisation
Théropode
Musaraigne

RÉSUMÉ

La morphométrie géométrique implique de définir des points homologues (*landmarks*) pour générer une représentation discrète d'un objet. Cette étape cruciale est fortement influencée par la problématique biologique guidant l'analyse, particulièrement avec les *semi-landmarks* de courbe et de surface qui nécessitent d'établir un gabarit (*template*) de référence. Nous illustrons ces contraintes avec deux jeux de données issus de sujets de recherche différents. Le jeu de données « théropode » est une analyse morphométrique fonctionnelle de bassins de théropodes actuels et fossiles présentant des formes très diversifiées. Le jeu de données « musaraigne » est une étude morphométrique populationnelle portant sur des différences ténues du crâne de la musaraigne musette. Nous proposons ainsi une nouvelle méthode pour concevoir un gabarit à configuration régulière, par modélisation polygonale. Elle permet le contrôle de la géométrie du gabarit pour adapter sa complexité à la variation morphologique dans l'échantillon. D'autres analyses concernant l'influence de la conception du gabarit devront établir l'intérêt de cette méthode aux niveaux morphométrique et statistique.

© 2010 Académie des sciences. Publié par Elsevier Masson SAS. Tous droits réservés.

1. Introduction

The quantitative study of biological shape through Geometric Morphometrics (GM) begins with the definition of structures of interest and of how they shall be represented by coordinates of landmark points. Landmarks are homologous points that must be found on each specimen and at the same time be relevant for the study. Recently, major breakthroughs in imaging and computing technologies have deeply impacted our approaches and conceptions in both the neontological and paleontological areas of biology. GM is directly regarded by such novel developments and morphometricians adopted these very early. Important theoretical and methodological advances quickly followed that have given birth to powerful new landmark-based investigation tools to analyse forms like curves and surfaces, that do not have discrete landmarks (Bookstein, 1997). As a consequence, the choice of the nature, number and localisation of landmarks must be particularly elaborate and influenced by the biological question(s) and the sampling strategy of the study.In this article, we show how two case studies can possibly lead to different methodological approaches using three-dimensional (3D) surface GM. To exemplify the points put forth in the text, we use preliminary results from research lead by two of us (TS and RC). These two analyses are particularly interesting in this context: the patterns of variability reported in both cases are quantitatively and qualitatively very contrasted. The first is a functional study on a very large evolutionary scale while the other deals with intrapopulational variation in a very homogeneous species of small mammals. Both make use of 3D scans on which were collected true landmarks as well as semi-landmarks. The use of semi-landmarks constrained onto curves and surfaces puts stress on the different nature of each study. We put particular emphasis on the choice of landmarks and construction of the template configuration, as the design of a good template is a time-consuming, critical step in this context (see "Geometric Morphometrics" and "Methods").

We begin by briefly introducing concepts related to 3D data and GM. We only provide a general overview of existing imaging devices, data acquisition methods as well as statistical treatments and visualisation possibilities offered by modern toolsets. For comprehensive historical reviews concerning GM, see Adams et al. (2004), Bookstein (1998), Rohlf and Marcus (1993) and Slice (2005). Readers will also find more details about GM approaches applied to 3D surfaces in two recent papers by Gunz et al. (2005) and Mitteroecker and Gunz (2009).

1.1. 3D acquisition

As shown in this volume, there is a diversity of methods for the acquisition of 3D morphological data and lower costs as well as greater ease-of-use make them more accessible. Though we do not provide a complete technical review, we want to specify the varied nature of the data provided by the different technologies, in the scope of a GM analysis.

There are three major types of systems allowing the acquisition of 3D data on a physical object. The first category, digitizers, includes optical, mechanical or handheld devices. These systems register data either via a probe or without contact. They usually collect point-by-point coordinates directly over the physical object–either by user selection or semi-automatically using geometrical criteria–with submillimetric to micrometric precision.

A second option is to acquire a 3D scan of the physical object and collect morphometric data on its digital representation via a software interface. There are two main types of 3D scanners. Surface scanners are optical contact-free devices using triangulation from projected structured light (laser lines, white light fringes) to produce a meshed 3D object. As a result, they exclusively provide a 3D representation of the visible external topology of objects. Their typical precision ranges from submillimetric down to around 10 μm, or even nanometers for laser-scanning confocal microscopy.

On the contrary, tomographic scanning permits to reconstruct the whole object, including its inner structures. It comprises different technologies using an inverse transform of multiple one-dimensional projections through an object to reconstruct a stack of virtual slices. Most common tomographic methods are X-ray Computed Tomography (CT scan), Synchrotron Radiation (SR) and Nuclear Magnetic Resonance Imaging (NMRI). Methods based on the

differential absorption of X-rays by materials of different densities are particularly used for scanning mineralized elements and fossils. The range of resolution goes from 0.5 mm to 5 μm in conventional CT and μCT scanners, and down to the nanometer with X-ray beams produced by SR. NMRI produces greatly detailed images of soft tissues. These tissues have a high and variable water content that allows NMRI to differentiate them, making it especially useful to reconstruct neurological, muscular, arthrological tissues or organs. Medical systems offer submillimetric resolution on a human body. For centimetric objects, higher spatial resolution is available from facilities held in research laboratories down to about 25 μm.

1.2. From 3D acquisition to Geometric Morphometrics data

The technology used for data acquisition will affect how 3D data should be processed prior to the morphometric analysis. Digitizers directly collect coordinates of points from the physical object. Hence, the data retrieved is usually ready for analyses by GM toolsets after little or no processing. As a counterpart, errors or modifications of the landmark configuration often imply to recollect data and hence to access the specimen again.

On the contrary, data registered from surface and tomographic scanners require tedious software postprocessing to obtain a 3D digital model of the specimen and collect morphometric data on it. High-resolution scans yield large amounts of data resulting in very dense point clouds. They require important decimation before export to morphometric software. Carefully selecting appropriate cleaning, alignment, merging and decimation options is critical in order to preserve the geometrical features of the original object in its digital model, while at the same time significantly reducing the memory load. Various software packages offer solutions to collect geometric morphometric data on the digital mesh model. Software for mesh processing or data visualisation (VSG Avizo Fire 6.1, http://www.vsg3d.com/; Geomagic Studio 11, http://www.geomagic.com/) provide tools to register point coordinates by hand or semi-automatically. A limited number of software packages, however, are explicitly oriented for 3D geometric morphometric data acquisition and/or processing and provide varying levels of user-friendliness (Edgewarp3D 3.31–Bookstein and Green, 2002; IDAV Landmark Editor–Wiley et al., 2005). Though scanning is time demanding, digital models have the advantage to allow for easy and fast correction or management of datasets as the morphometric acquisition step can be saved in a file, to be reopened and edited.

At this point, we highlight that all these methods result in a representation of the structure(s) of interest made of discrete 3D landmark coordinates, likely to be used in quantitative analyses of shape variation.

1.3. Geometric Morphometrics

The 'template' is a landmark configuration used as the reference for any new specimen added to the study. It is composed of every landmark used in the analysis with its associated type–true landmark and either curve or surface semi-landmark. The choice of the type, number and relative location of landmarks is hence a critical step in creating a template configuration, that is highly influenced by the aim of the study and the nature of the sample.

Homologous ("true") landmarks define a direct correspondence between parts of different objects: homology is in this case not the biological homology, but a geometrical one (sensu Jardine, 1969). True homologous landmarks belong to the types I and II of Bookstein (1991) that correspond to juxtapositions of tissues and maxima of curvatures respectively. By opposition, type III corresponds to weakly defined points (the more distant from a reference by instance) and to outline points. Both are regrouped into the name of semi-landmark that recalls that they are defined only in one direction and that some of their coordinates are deficient (Bookstein, 1997; Gunz et al., 2005).

Semi-landmarks demand different approaches than true landmarks to be used in shape comparisons. Two strategies can be employed.

In the first procedure, introduced by Bookstein (1997) (see also Gunz et al., 2005), non-homologous landmarks can be transformed into operational landmarks using geometrical and mathematical criteria. This is achieved by allowing them to slide, whether along predefined curves or on surfaces, while optimizing a criterion such as minimizing the bending energy parameter used by the thin plate splines (Bookstein, 1997; Gunz et al., 2005; Mitteroecker and Gunz, 2009). True homologous landmarks are mixed with non-homologous ones in order to introduce spatial constraints (Gunz et al., 2005). At the end of the process, all landmarks, whatever their types, are superimposed and treated in the same way true homologous landmarks are. To perform this operation, curve and surface semi-landmarks must be transferred from the template configuration onto the target specimen by 'warping'. In this procedure, the new target specimen is defined by its true landmarks coordinates. Based on this different configuration of true landmarks, the thin plate spline is a one-to-one spatial interpolation function that warps semi-landmarks into their new position. Once warped, semi-landmarks must be projected onto their respective target curves and surfaces to proceed to spline relaxation. Finally, as explained in detail in Gunz et al. (2005), semi-landmark sliding must be repeated iteratively using each newly formed consensus until convergence is attained.

A second approach uses mathematical functions to directly describe the whole set of points. This has been done with 2D and 3D outline points (see Figs. 1 and 2 for examples of 3D outlines) by using, for example, Fourier decompositions (Baylac and Friess, 2005; Ferson et al., 1985; Kuhl and Giardina, 1982) or eigenshape analysis (McLeod, 1999). At one point, steps are included that allow for some form of registration, including size normalisation, either of the raw coordinates or directly applied to the function parameters (Kuhl and Giardina, 1982). At the end of the process, the parameters of the functions are used as shape variables in the statistical analyses. Invertible functions have been favoured since their parameters may be

used to reconstruct the shapes allowing for straightforward visualisations of the shapes.

For homologous and sliding landmarks, a single morphometric operation, the Procrustes superimposition (Rohlf and Slice, 1990) is used to provide a common referential system that makes point coordinates comparable. This step is necessary because, unlike distances, point coordinates are not invariant to the simple geometric operations of translations and rotations: measured distances remain identical if one translates and rotates the objects, whereas point coordinates do not. The superimposition procedure will eliminate from the original coordinates the components related to the translations and rotations, adding a further size normalisation operation. Mathematically, this superimposition operation minimises the overall sum of squares between all homologous landmarks of a set of objects. Geometrically, it is a translation and a solid rotation of each object toward a reference object, usually iteratively calculated as the mean object or consensus. The result will be a set of superimposed landmark coordinates that have the same size and that summarize the geometrical differences between objects. The superimposition process therefore realizes the extraction of size and shape (here the superimposed coordinates) terms from the overall form of an object, following Needham's (1950) equation: form = size + shape. These size and shape terms may be simply visualized but more interestingly can be subjected to multivariate statistical analyses (Dryden and Mardia, 1998; Krzanowski, 1988).

Size normalisation is done by dividing each set of point coordinates of an object by its size. Size is estimated by the centroid size (Bookstein, 1991), the square root of the sum of squared distances between the centroid of an object and its landmarks. Superimposed coordinates are therefore ratios and size normalisation corresponds to a simple scaling step, that leads to objects of uniform size but does not modify their individual proportions. Nevertheless, biologically, size and shapes are rarely independent. Moreover, their relationships define one important component of the biological variability, namely the allometries (see Klingenberg, 1996). Readers interested by the important conceptual and practical consequences of the use of ratios are referred to Darroch and Mosimann (1985), Mosimann and James (1979) and Bookstein (1996) together with Small (1996) and Dryden and Mardia (1998), which introduce the complexity of shape spaces (see also Rohlf, 2000 for useful and visually illuminating examples).

1.4. Statistical analyses and visualisations

For some reasons, detailed in Gunz et al. (2005, pp. 86–88), statistical inferences using semi-landmarks, whether of the surface or of the ridge type, are not a simple straightforward extrapolation of the usual inferences done using the Procrustes coordinates. Nevertheless, exploratory analyses like Principal Components Analyses (PCA) or Partial-Least-Squares (PLS) are always feasible. In this article, the description of the shape variability uses exclusively PCA.

The value of GM does not only reside in its great statistical power. It also resides in the simple yet powerful visual interpretations it provides. Visualisations may be simply direct comparisons of superimposed shapes. More generally, the analyses of shape variability are frequently done in relation to predefined factors (size in the case of allometry, groups of objects, archaeological beds, palaeontological strata, ecological or environmental parameters) that may be related to particular directions of variability into the shape space. Alternatively statistical directions like factorial axes, principal components or canonical axes may be also specifically calculated from the shape covariance matrices. Visualisations may also be done along the directions of maximum variances between one set of shape parameters and one set of variables of interest using 2-Blocks Partial Least-Squares (2B-PLS; Rohlf and Corti, 2000). This permits analysis and visualization of shape changes associated with a set of variables characterising past or present environments, ecotones, ecological niches, functional or physiological parameters (Adams and Rohlf, 2000).

All these visualizations of either 2D or 3D landmarks and semi-landmarks estimate the statistical relationships between shape and the specific directions of interest (DOI) using multivariate regression (Dryden and Mardia 1998; Monteiro, 1999). By this methodology, the particular landmark configuration that corresponds to a single value picked along the DOI may be calculated and visualized. Usually both extremities along the DOI are contrasted to illustrate the overall shape differences (see "Results"). Multivariate regression is useful whatever the nature of the variables is: landmarks, semi-landmarks, outline or surface function parameters. In the case of a shape described by parameters of mathematical functions, the inverse function allows for the calculation and visualization of the coordinates of reconstructed shapes.

2. Materials

2.1. The theropod dataset

The first dataset deals with large scale evolution and locomotory adaptations among extinct and extant theropod dinosaurs (bipedal, generally carnivorous; including birds). The history of this diversified group dates back to Carnian (Late Triassic > 230 My) and covers major geological and evolutionary events. Bipedalism was present since the origin of Theropoda (and perhaps other Dinosauria), while the > 9500 species of modern birds today remain the sole obligatory, striding bipeds with the exception of humans. Moreover, their terrestrial locomotor apparatus maintained an overall similar organisation, though it underwent a gradual sequence of modification that has motivated numerous studies of anatomy and function (Gatesy, 1995; Hertel and Campbell, 2007; Hutchinson, 2001; Hutchinson, 2004a; Hutchinson, 2004b; Hutchinson and Gatesy, 2000; Rasskin-Gutman and Buscaglioni, 2001; Reilly, 2000; Rubenson et al., 2007).

The aim of the broader study is to analyse shape variation of the pelvic girdle with a focus on the geometry of hip joint and antitrochanter (articular surface adjacent to the acetabulum, Fig. 1). To investigate how hip form and function evolved, the sample must be representative of

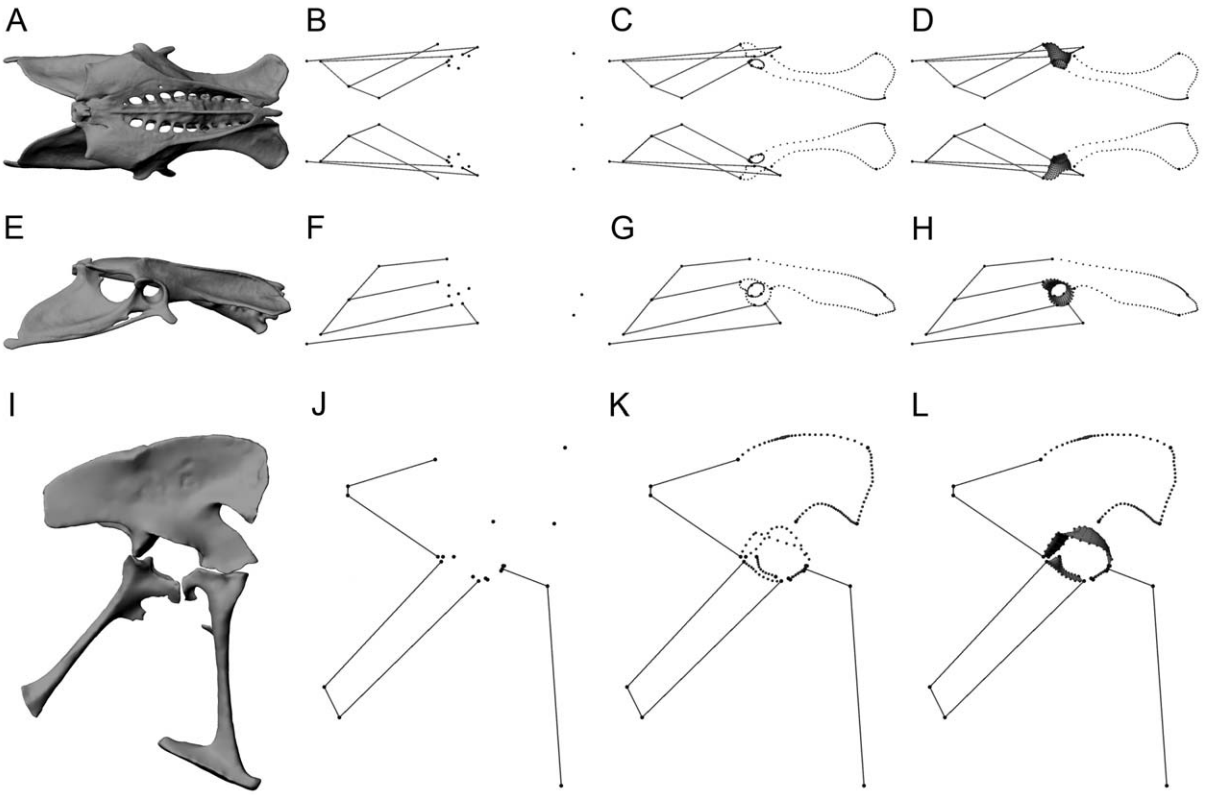

Fig. 1. Location of the 936 landmarks and semi-landmarks on the pelves of the Theropod Dataset, for *Coturnix* (quail) in dorsal (A, B, C, D) and right lateral view (E, F, G, H) and *Allosaurus* in right lateral view (I, J, K, L). We present 3D scans of the pelves (A, E, I) together with corresponding configurations of true landmarks (B, F, J), true landmarks with curve semi-landmarks (C, G, K) and true landmarks with curve and surface semi-landmarks (D, H, L).
Fig. 1. Localisation des 936 *landmarks* et *semi-landmarks* sur les bassins du *Theropod Dataset*, pour *Coturnix* (caille) en vue dorsale (A, B, C, D) et latérale droite (E, F, G, H) et pour *Allosaurus* en vue latérale droite (I, J, K, L). Nous présentons les *scans* 3D des bassins (A, E, I) associés aux configurations correspondantes de « vrais » *landmarks* (B, F, J), de « vrais » *landmarks* et *semi-landmarks* de contour (C, G, K) et de « vrais » *landmarks* et *semi-landmarks* de contour et de surface (D, H, L).

the morphological, ecological and taxonomical diversity found among Theropoda. Hence, this dataset is remarkable because of the important variability it comprises. As a result, finding homologous landmark locations can be problematic and no single specimen can accurately represent the morphology of all others to create a template configuration (Fig. 1).

To illustrate such analysis, the Theropod Dataset presented here comprises 3D models of five pelvic girdles (*os coxae*). Extant animals are represented by four randomly selected genera of modern birds belonging to three different clades: *Coturnix* (Phasianidae, Galliformes), *Calonetta* (Anatidae, Anseriformes), *Troglodytes* (Troglodidae, Passeriformes) and *Taeniopygia* (Estrildidae, Passeriformes). These genera range from very small (9 cm long, 10 g) to small (20 cm long, 180 g) birds. Models were obtained using X-ray microtomography, with isometric voxel resolutions ranging from 22 μm to 64 μm. Segmentation was performed using Avizo (VSG Avizo Fire 6.1).

Allosaurus fragilis is the only representative of non-avian theropods included in this study. Scanning was performed at the Museum of the Rockies on fossil specimen MOR 693 ('Big Al') with a Modelmaker scanner and postprocessed with Paraform Viewer.

We placed a total of 936 landmarks on each specimen (Fig. 1): 44 anatomical landmarks, 280 sliding semi-landmarks on 3D curves and 612 sliding semi-landmarks on 3D surfaces. Anatomical landmarks were placed on homologous locations delimiting the overall shape of the pelvis, as well as circumscribing the endpoints of curves. The curves represent clearly defined ridges, either delimiting the extent of the preacetabular ilium or the articular surface of the acetabulum and antitrochanter. Surface sliding semi-landmarks form a dense mesh over the articular facets of both hip joints.

2.2. The Shrew Dataset

The second dataset deals with skull evolution in populations of shrews. One of the most noticeable particularities is the homogeneity of their global form across time and geography (Churchfield, 1990). Among shrews, *Crocidura russula* is morphologically wellconserved throughout its geographical range. However, previous studies using 2D GM on French populations showed tiny but significant morphological differences related to geography in general and insularity in particular.

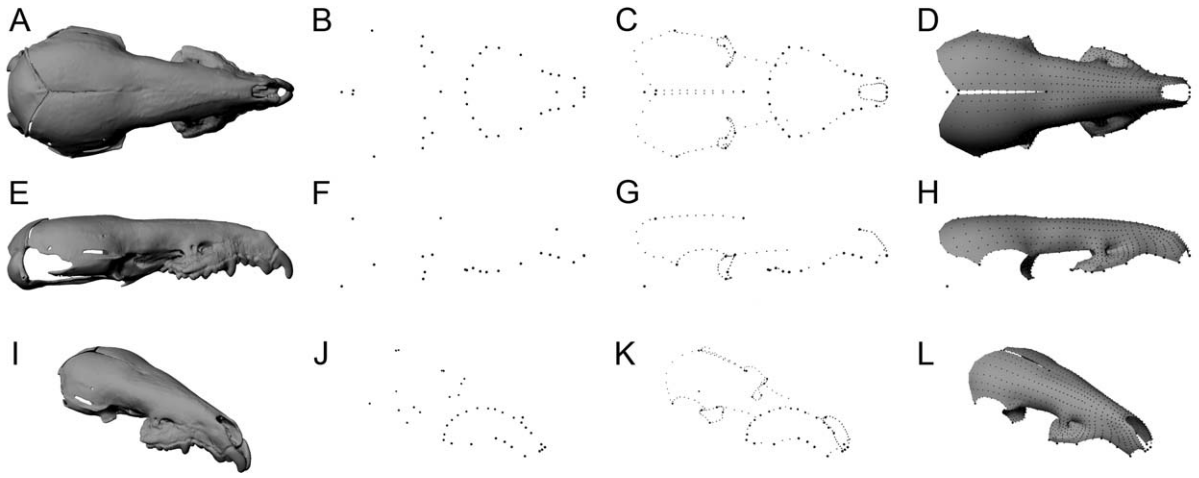

Fig. 2. Location of the 996 landmarks and semi-landmarks on the skulls of the Shrew Dataset, in dorsal (A, B, C, D), right lateral view (E, F, G, H) and perspective view (I, J, K, L). We present a 3D scan of the skull (A, E, I) together with corresponding configurations of true landmarks (B, F, J), true landmarks with curve semi-landmarks (C, G, K) and true landmarks with curve and surface semi-landmarks (D, H, L).
Fig. 2. Localisation des 996 *landmarks* et *semi-landmarks* sur les crânes du *Shrew Dataset*, en vue dorsale (A, B, C, D), latérale droite (E, F, G, H) et perspective (I, J, K, L). Nous présentons un *scan* 3D de crâne (A, E, I) associé aux configurations correspondantes de « vrais » *landmarks* (B, F, J), de « vrais » *landmarks* et *semi-landmarks* de contour (C, G, K) et de « vrais » *landmarks* et *semi-landmarks* de contour et de surface (D, H, L).

The aim of the current study is to characterise and quantify more precisely morphological variations on the whole skull (Fig. 2) using 3D surface GM in order to explain these variations linked to genetics or/and environmental factors.

This dataset is remarkable because different specimens are very similar and potential differences very tiny. Nevertheless 3D surface GM allow us to describe both globally the form of the skull and specifically the different regions of the skull involved in sensory functions like the ocular, the auditory, the nostril or the masticatory regions. Another consequence is that one specimen can potentially be used to create a template configuration efficient for the whole dataset.

To give an example of such application, the Shrew Dataset is composed of five specimens from five different populations. These specimens have been scanned using X-ray microtomography with a resolution of 20 μm. As for the precedent dataset, data have been segmented with Avizo (VSG Avizo Fire 6.1).

996 landmarks have been used to describe the skull. Most of them are spread over the dorsal side (Fig. 2). They consist of 39 anatomical landmarks, 157 sliding semi-landmarks on 3D curves and 800 sliding semi-landmarks on 3D surfaces. Most anatomical landmarks correspond to intersections of different bones or teeth and can be considered to belong to type "1" homologous landmarks, according to Bookstein (1991). Curves are located at the periphery of large bones like the parietal, maxillar and nasal. Sliding semi-landmarks on 3D surfaces were placed over the dorsal part of the skull from the nasal to the parietal bones, where no true landmarks could be found. Semi-landmarks were also used to describe the mandibular fossa region which, as most articular surfaces is devoid of any true landmarks.

All these choices have been done regarding two aims, first to describe the global form of the skull by a relatively dense covering of semi-landmarks, and second to deal with regional part of interest of the skull, most of them corresponding to sensitive regions.

3. Methods

3.1. Landmark choice and template design

As the Generalised Procrustes Superimposition (GPA) relies on a landmark-based discrete representation of biological shape, the design of an appropriate template is a crucial step in the workflow. It is pointed out by Gunz et al. (2005) that this definition of the relative location and repartition will dominate the resulting statistical processing and visualisation of the data.

In their paper, Gunz et al. (2005) explain how they proceed to obtain the landmark configuration that is used as the template. To do so, they use a randomly chosen specimen of their sample as reference. True landmarks and curve semi-landmarks are digitized directly onto it, while surface semi-landmarks are obtained from a dense point cloud digitized on the specimen. Decimation–controlled reduction of the number–of the redundant points of this cloud produces a more sparse and relatively regular pattern that can be used as surface semi-landmarks. As they specify, similar results can be obtained by using the dense mesh resulting from surface or volume scanning.

In our case, the different nature of the two dataset requires different approaches for the design of each template configuration. This leads to the introduction of a novel method to design templates for sliding semi-landmark GM analysis, adaptable to the level of shape variability in the sample. During the warping of the template onto the target specimen, as the configuration of true landmarks interacts with semi-landmarks, much of the original geometry of the template is retained for curve and surface semi-landmarks. As a result, for semi-landmarks located on morphological features geometrically similar on the template and the

target, warping will efficiently bring them close to the homologous target area. This proves particularly useful in the case of samples with very homogeneous specimen morphologies, as little to no hand processing has to be performed after warping, before to project and slide the semi-landmarks. On the contrary, for features with significantly different shape on both objects, warping may leave the semi-landmarks relatively far from the target area they should be projected on. These cases require difficult and time-consuming hand processing to correct the position of offset semi-landmarks and attain a satisfying match onto the target specimen, so that the semi-landmarks can be correctly projected and relaxed.

As previously noted, contrarily to the Shrew Dataset, no single specimen from the Theropod Dataset displays morphological properties that can efficiently be warped into the geometry of every other specimen. Hence, we designed both templates using polygonal modelling tools in Maya (Autodesk® Maya 2010) to create each template with a different level of geometrical complexity. With this method, instead of designing the Theropod Dataset template on one random specimen, we were able to create it with a much lower level of complexity (Fig. 3). It was modelled using simple 3D geometrical primitives–planes, cylinder–and controlled modelling tools, to produce a basic idealised shape with equidistant curve semi-landmarks and grid-like surface patches. Because the template shape is less complex, warping the semi-landmarks retains simpler geometrical features. As a direct benefit, fewer and faster manual adjustments are required before the warped semi-landmarks closely match their new target position.

On the other hand, the Shrew Dataset presents a very homogeneous form. Hence, we could model a reference mesh with greater geometrical complexity based on the morphology of a specimen of the dataset (Fig. 3). As a result, we obtained a template that can easily be warped and projected onto other target specimens, in a similar way to what is proposed in Gunz et al. (2005). However, polygonal modelling has other benefits as it provides direct control over the number and the individual location of semi-landmark points. Moreover, the simple tools used to add or refine divisions and vertices allow one to create very regular tessellations with evenly spaced points covers. This modelling of the reference mesh into a regular pattern permits an efficient management of local point density (Fig. 3) and to subdivide the template into regions of interest for further analysis. The differences in the warping step resulting from the distinct approach used for each dataset are illustrated in Fig. 4.

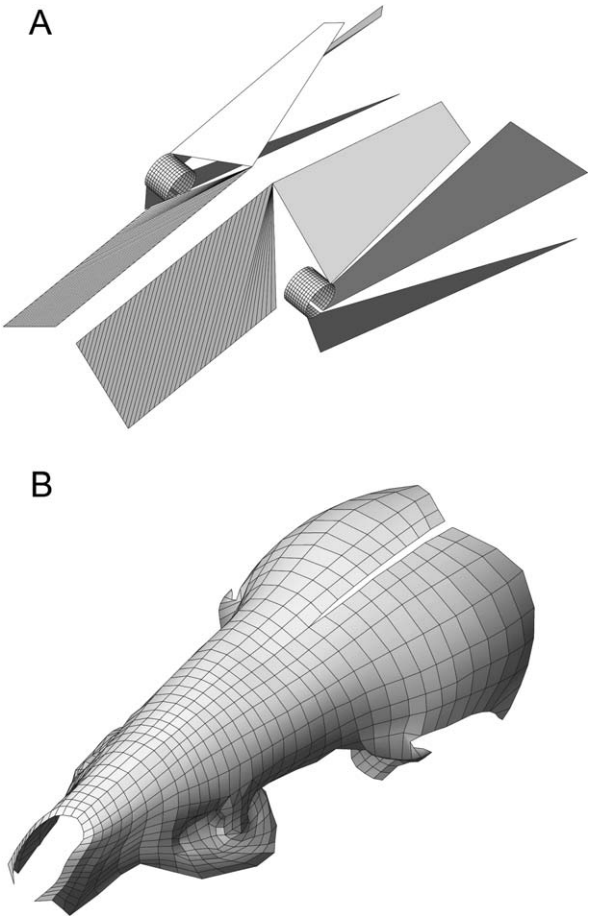

Fig. 3. Template configurations used for the initial warping step for the Theropod Dataset (A) and Shrew Dataset (B). Models are created using polygonal modelling tools in Maya (Autodesk® Maya 2010). The mesh vertices are lying at each edge intersection. These points are then converted into true landmarks, curve and surface semi-landmarks. A different amount of geometrical complexity is used for each template in relation to the amount of morphological variation in each dataset (see Figs. 1 and 2).
Fig. 3. Configurations des *templates* utilisés dans l'étape de *warping* initiale pour le *Theropod Dataset* (A) et le *Shrew Dataset* (B). Les modèles sont créés à l'aide d'outils de modélisation polygonale dans Maya (Autodesk® Maya 2010). Les « vertices » (*sommets*) se trouvent à chaque intersection d'arêtes. Ces points sont ensuite convertis en « vrais » *landmarks* et *semi-landmarks* de courbe et de surface. Des niveaux différents de complexité géométrique sont utilisés pour chaque *template* relativement à l'ampleur de la variation morphologique dans chaque jeu de données (voir Fig. 1 et 2).

3.2. Morphometric and statistical analyses

We use Edgewarp3D 3.31 (Bookstein and Green, 2002) to warp our reference configuration onto each specimen and perform iterative semi-landmark relaxation to their final target positions. Fig. 4 illustrates this step for both datasets. After an initial Procrustes superimposition and computation of a consensus configuration, semi-landmark sliding is iteratively repeated using the new computed consensus as template until convergence is obtained (Gunz et al., 2005). The resulting data is exported to perform GM in the graphical and statistical R environment (http://cran.r-project.org/) using the Rmorph library (MB). Each dataset is then superimposed using a Generalized Procrustes Analysis. Objects are made symmetrical using the procedure for object symmetry of Mardia et al. (2000). Superimposed coordinates are subjected to an unscaled Principal Component Analysis (PCA). Visualization are done using multivariate regression and links between selected points are defined in order to help visualize the objects. The results are used to produce warped surfaces and visualisations using two programs, namely SurToPly and ColorMorphoPly, which are still in ongoing development by one of us (J.P.).

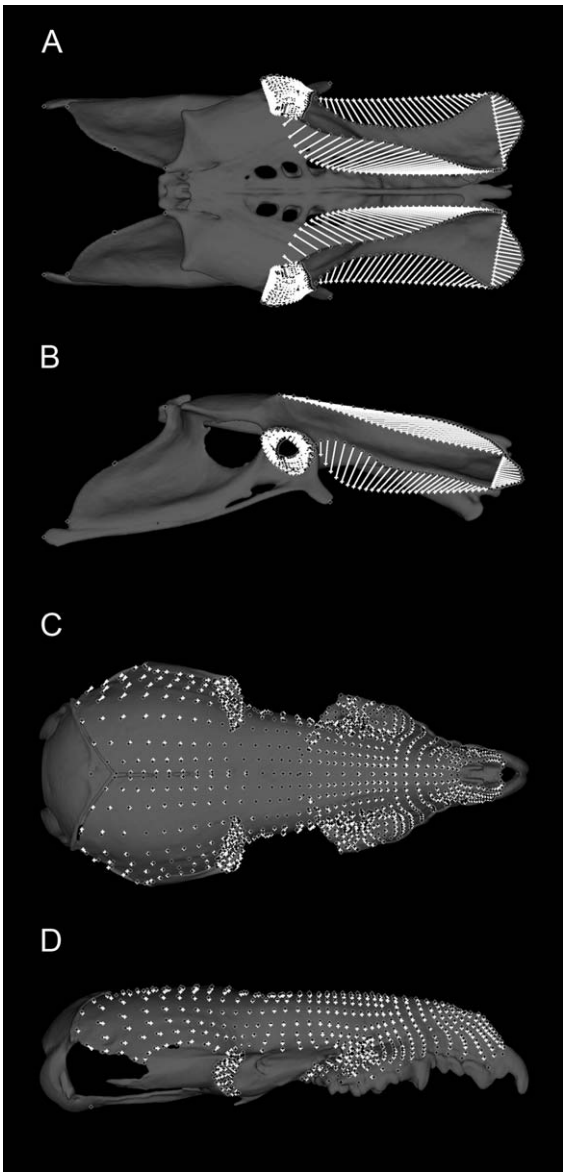

Fig. 4. Semi-landmarks warping, projection and relaxation is illustrated for *Coturnix* (A, B–Theropod Dataset) and *Crocidura* (C, D–*Shrew Dataset*). Initial semi-landmarks position (white crosses) after warping the template configuration is compared with their ultimate position (black crosses) after iterative projection and relaxation ('sliding') onto the target object. Differences between initial and ultimate position (white lines) are important when shape shows strong variation (A, B–Theropod Dataset) relative to cases with small variations (C, D–Shrew Dataset). Data is displayed by Edgewarp 3.31 (Bookstein and Green, 2002) and mapped over semi-transparent 3D scans for visual assistance.

Fig. 4. Illustration du *warping*, de la projection et de la relaxation des *semi-landmarks* pour *Coturnix* (A, B–*Theropod Dataset*) et *Crocidura* (C, D–*Shrew Dataset*). La position initiale des *semi-landmarks* (croix blanches) après *warping* de la configuration *template* est comparée avec leur position finale (croix noires) après projection et relaxation itératives (« sliding ») sur l'objet cible. Les différences entre positions initiale et finale (lignes blanches) sont importantes, lorsque la morphologie est très variée (A, B–*Theropod Dataset*) en comparaison des cas de faible variation (C, D–*Shrew Dataset*). Les données sont visualisées dans Edgewarp 3.31 (Bookstein et Green, 2002) et surimposées à des *scans* 3D semi-transparents pour fournir une assistance visuelle.

4. Results

4.1. The theropod dataset

Unsurprisingly, the first PCA axis (81.77% of variance) separates the avian from the non-avian Theropoda, while the second PCA axis (13.49% of variance) describes the avian variation. The interpretations that can be made from such results are however interesting.

Shape variation for PC1 (Fig. 5) ranges from a minimum very close to the non-avian *Allosaurus* specimen, to a maximum displaying a mix of all four birds' attributes. This results in a relative shortening and dorsoventral compression of the preacetabular ilium, which turns from a flexed, laterally facing lateral position to a straighter, dorsally facing medial one as we move along PC1. The postacetabular ilia experience a prominent proportional lengthening, as they simultaneously widen from a dorsomedial position to a ventrolateral one. Concerning ischia, differences put forth by Procrustes superimposition reveal a relative shortening and shift from a highly medial to a fully lateral, more ventral orientation corresponding to the positive extreme of PC1. The distal pubic symphysis separates as the pubes retrovert and expand laterally alongside the ventral edge of the ilia. More generally, these results also demonstrate that non-avian theropods (i.e. *Allosaurus*, which is reasonably representative of most taxa) have a relatively narrow pelvis, wider at the cranial tip of the ilia, whereas birds have a relatively wider pelvis that proportionally widens toward its caudal end. Thus our methods quantitatively capture changes that have been fairly well described in qualitative anatomical descriptions (e.g. Hutchinson, 2001; Hutchinson and Gatesy, 2000).

The hip experiences rather dramatic changes (Fig. 5 C, D, E). Acetabular cavities are found into a proportionally much more lateral position on the positive–avian–side of the axis. The acetabular opening also is proportionally much larger on the *Allosaurus* side of PC1 relative to the four extant birds, and this mainly involves relative displacements from the ventral halves of the iliac and ischial articular facets and from the pubes. Noticeably, along PC1 the dorsal iliac part of the acetabulum reduces mediolaterally.

The minimum of PC2 (Fig. 6) lies very close to *Coturnix* and the positive end of the axis lies relatively close to *Troglodytes* and *Taeniopygia*. This corresponds to a change in the shape of the preacetabular ilia from a slender, elongate outline with a broaden cranial extremity on the quail side, to a proportionally shorter, higher dorsoventrally shape with a wider base on the positive extreme of the axis. Deformation along this Principal axis shows a relative shortening of postacetabular iliac blades as they reorient in a more dorsolateral direction. Also, the ischia become slightly larger and spread relatively farther laterally on the positive extremum. Toward the positive end of the PC2 axis, the pubes relatively face more cranially, and also more laterally, though less than is observed in the ischia.

The pattern of changes occurring within the acetabulum along PC2 (Fig. 6 C, D, E) is less exaggerated than that displayed by PC1, but nonetheless may have appreciable functional importance. We observed some variation in the size of the acetabular cavity, with the PC2 minimum

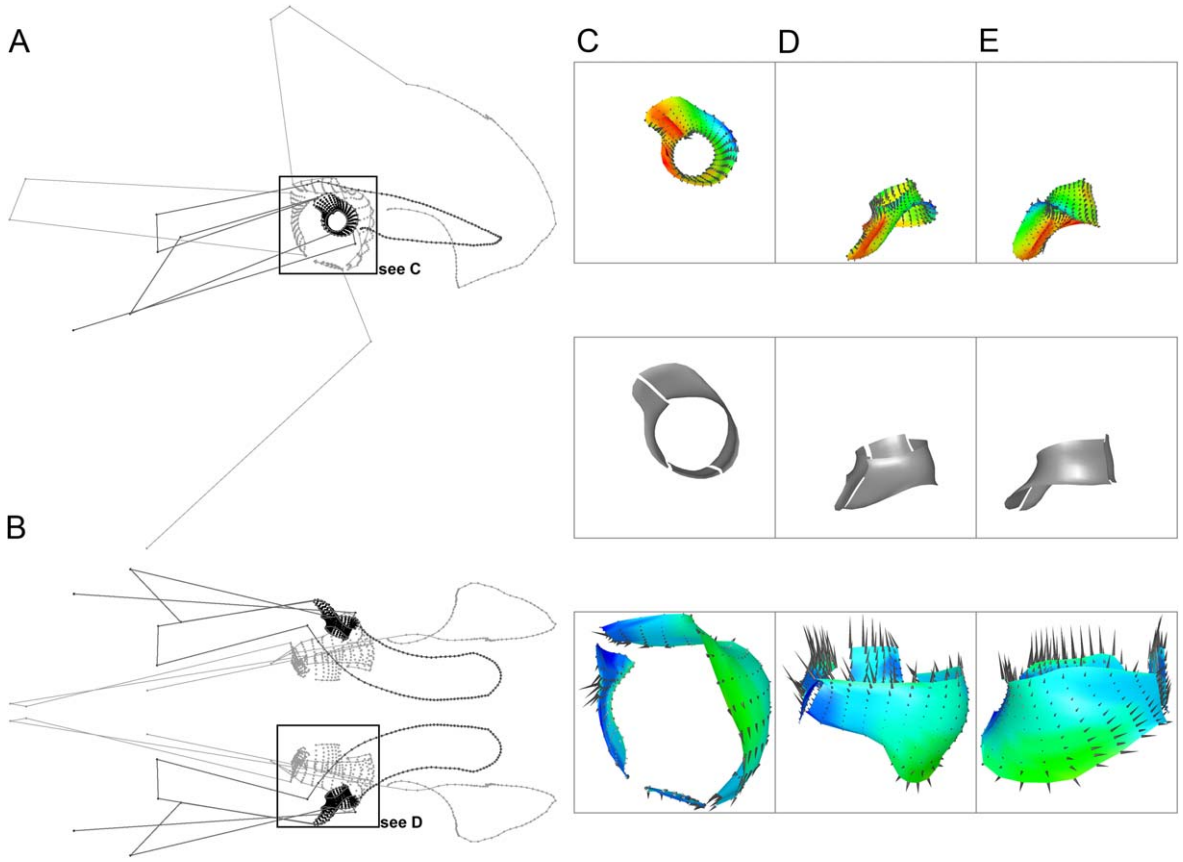

Fig. 5. Shape variation along PCA axis 1 of the Theropod Dataset. Extreme shapes for the negative side (light grey) and positive side (dark grey) are represented in right lateral (A) and dorsal (B) view. The right panel (C, D, E), shows detailed surface visualisations of acetabular deformation along PC1, in right lateral (C), dorsal (D) and cranial (E) view. The consensus (centre row) is figured between the minimum (bottom row) and maximum (top row) shape along PC1. Visualisation: to help for visual interpretation, deformation vectors are decomposed into their respective normal and tangent components relative to the consensus surface. Grey arrows indicates the direction and magnitude of deformation occurring along the consensus surface, the pattern of colour temperature indicates the direction and magnitude of deformation perpendicular to the consensus surface: green indicates null normal deformation, warm colours indicates positive normal deformation component (outward) and cold colours indicates negative normal deformation (inward).
Fig. 5. Variation des conformations le long de l'axe 1 de l'ACP pour le *Theropod Dataset*. Les extrêmes du côté négatif (gris clair) et positif (gris foncé) de l'axe sont représentés en vue latérale droite (A) et dorsale (B). Le panneau de droite (C, D, E) montre en détail les déformations de la surface acétabulaire le long de PC1, en vue latérale droite (C), dorsale (D) et crâniale (E). Le consensus (ligne centrale) est figuré entre le minimum (ligne inférieure) et le maximum (ligne supérieure) sur PC1. Visualisation : afin d'assister l'interprétation visuelle, les vecteurs de déformation sont décomposés en composantes normales et tangentes relativement à la surface consensus. Les flèches grises indiquent la direction et la magnitude des déformations tangentes le long de la surface consensus, la température des couleurs indique la direction et la magnitude des déformations perpendiculaires à la surface consensus : la couleur verte indique une déformation normale nulle, les couleurs chaudes indiquent les composantes normales des déformations positives (vers l'extérieur) et les couleurs froides indiquent les déformations normales négatives (vers l'intérieur).

involving a hip with a much smaller relative diameter. There are also noteworthy changes in the orientation of the acetabular opening. On the negative end of PC2, the medial outline of the articular surface is smaller and shifted caudodorsally, resulting in a more conical opening, facing ventrolaterocranially when compared to the wider, laterally facing and more cylindrical acetabulum of the positive end. Finally, the antitrochanter also exhibits major changes. It is also less well-developed and attached only to the caudodorsal quarter of the acetabular lateral ridge on the negative end, while it is very wide and attaches over almost the entire caudodorsal half of the acetabulum on the positive side. In doing so, it ends up shifting into a relatively more dorsal orientation along PC2.

4.2. The Shrew Dataset

Fig. 7 represents 3D surface differences of shape along the first axis of an example of PCA realised on specimens of different geographical origin representing 38.6% of total variability. We can visualize the variable regions of the skull in 3D with a colour code. Four main examples of interpretation have to be noted.

First, the nasal part, related to olfactory sense and food foraging, is different along this axis and seems to be proportionally smaller on the positive part of the axis regarding the blue colouration of this region. This pattern may be interpreted in terms of adaptive traits of difference of olfactory capacity.

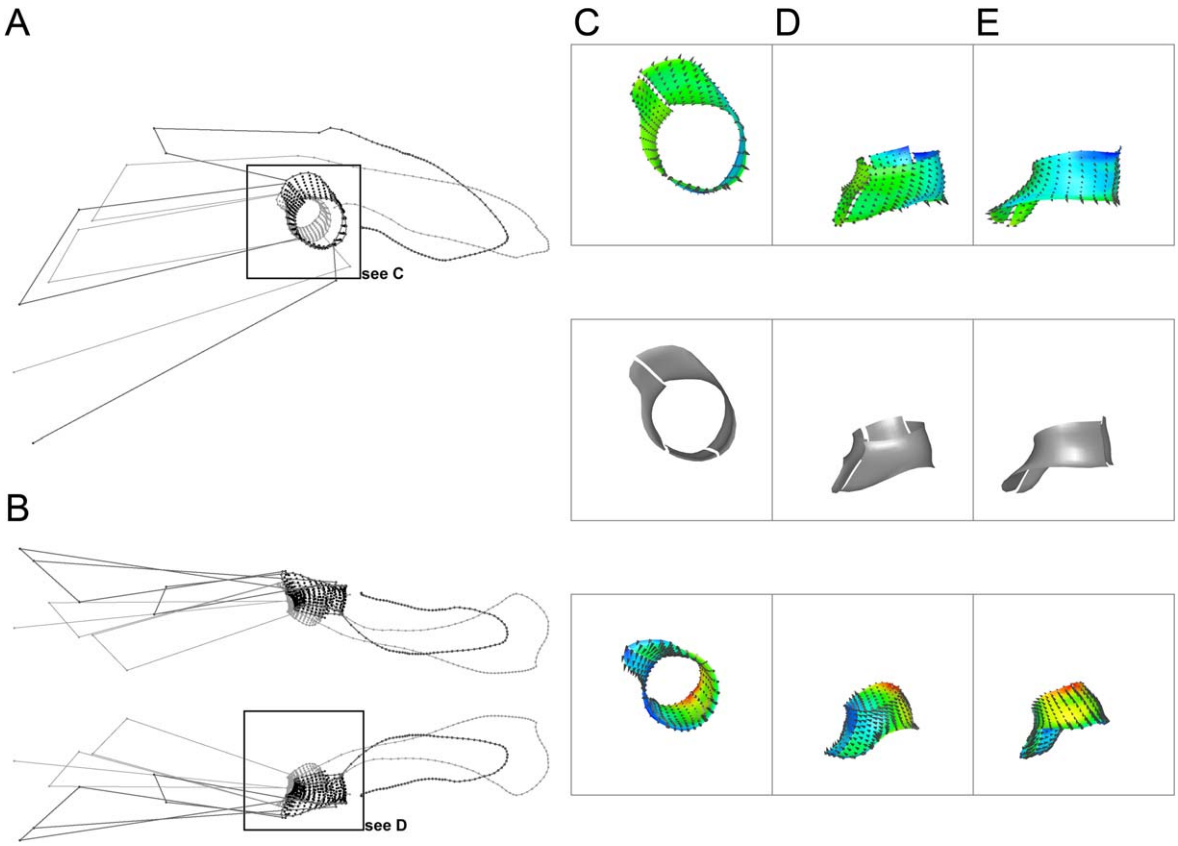

Fig. 6. Shape variation along PCA axis 2 of the Theropod Dataset. Extreme shapes for the negative side (light grey) and positive side (dark grey) are represented in right lateral (A) and dorsal (B) view. The right panel (C, D, E), shows detailed surface visualisations of acetabular deformation along PC2, in right lateral (C), dorsal (D) and cranial (E) view. The consensus (centre row) is figured between the minimum (bottom row) and maximum (top row) shape along PC2 (Visualisation: see caption of Fig. 5).

Fig. 6. Variation des conformations le long de l'axe 2 de l'ACP pour le *Theropod Dataset*. Les extrêmes du côté négatif (gris clair) et positif (gris foncé) de l'axe sont représentés en vue latérale droite (A) et dorsale (B). Le panneau de droite (C, D, E) montre en détail les déformations de la surface acétabulaire le long de PC2, en vues latérale droite (C), dorsale (D) et crâniale (E). Le consensus (ligne centrale) est figuré entre le minimum (ligne inférieure) et le maximum (ligne supérieure) sur PC2 (Visualisation : voir la légende de la Fig. 5).

Second, a depression localised at the junction of the frontal and parietal bones distinguishes specimens along this axis.

Third, the overall form of the braincase is more or less convex and longer according to the origins of the specimens. Indeed, specimens situated on the positive part of the first axis have a proportionally longer braincase than specimens situated on the negative part which have a more globular braincase.

Fourth, the two mandibular fossa present variations that could be revealing different diets through chewing mode. In this case, these differences can be regarded in term of geometry (convexity, orientation of the articular surface) and related to the associated movement of the mandible. These last two different patterns of shape are clearly demonstrated along this axis even if further studies are needed to explain it.

5. Discussion and conclusions

In the context of this article, results should not be over interpreted. As stated in the "Introduction" they are exploratory and based on minuscule samples. We use them to illustrate the use and benefit of such methodology in two very distinct cases of shape variation.

Indeed, the type of biological question should lie at the core of any decision, from the nature of the morphometric measurements to the acquisition method and device. This later aspect is often overlooked because of the technical constraints it imposes, but much of the significance of the dataset will depend on the reliability of raw scannographic data and its processing. An important benefit from working on a digital model is the possibility to reopen, edit and export morphometric measurements without having to reaccess the physical specimen and collect another complete dataset.

We advocate the benefits of 3D surface GM in cases very diverse, as those illustrated by our datasets. By mapping a dense mesh of points over homologous areas this method provides an excellent description of the overall shape of complex biological structures. This is particularly evident for the Shrew Dataset (Figs. 2 and 7) in which the cover of surface semi-landmarks allows for very precise description and visualization of the whole skull shape differences.

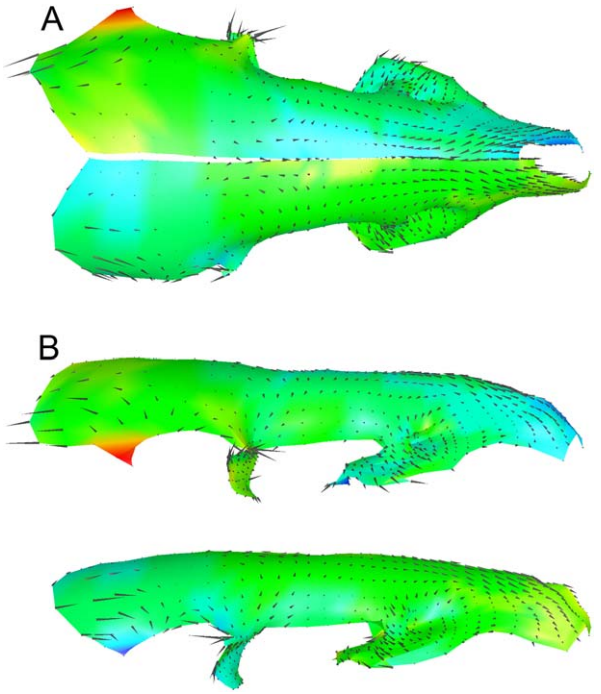

Fig. 7. Shape variation along PCA axis 1 of the Shrew Dataset. Surface representations in dorsal (A) and right lateral (B) views show extreme shapes for the negative side (bottom) and positive side (top) of PC1. (Visualisation: see caption of Fig. 5).
Fig. 7. Variation des conformations le long de l'axe 1 de l'ACP pour le *Shrew Dataset*. Les représentations de surface en vues dorsale (A) et latérale droite (B) montrent les extrêmes du côté négatif (ligne inférieure) et positif (ligne supérieure) de PC1. (Visualisation : voir la légende de la Fig. 5).

At the same time, however, the number of semi-landmarks densely spread over curves and surfaces is also able to characterise very local or modular differences with great accuracy. This is visible on Fig. 7 for the Shrew Dataset, and even more dramatically in the Theropod Dataset from magnified views of the acetabular deformation along the principal axes (Fig. 5 C, D, E and Fig. 6 C, D, E).

The main advantage, as put forth in Bookstein (1997), is the capacity of this method to work on biologically homologous regions without landmarks. Indeed, a significant amount of morphological variation occurs in areas where no discrete landmark-based representation can be placed. This type of variation is typically found in articular facets or in the middle of large bones of the brain case. This is well illustrated by the shape variation of the acetabular surface and iliac curves in the Theropod Dataset (Figs. 5 and 6) and of the parietal bone in the Shrew Dataset (Fig. 6), which in both cases represents an important part of the overall variability.

Finally, we propose a novel method to design templates that appears reliable for sliding semi-landmark GM analysis with samples involving variable amounts of variation. As a first step, it is crucial to carefully define the relative location and density of true landmarks as well as curve and surface semi-landmarks, necessary for the analysis by studying various specimens. We illustrate the benefits of constructing template configurations using 3D polygon modelling and how it can be adapted to very different cases (Fig. 3).

Many methods are proposed to generate template configurations. Automatic remeshing methods based on algorithms that iteratively optimise mesh parameters only give partial control over the resulting template geometry. By performing controlled operations like ridge detection, decimation, smoothing or minimum angle maximisation, these procedures can efficiently produce regular meshes composed of evenly spaced, isotropic or curvature based point covers. Nevertheless, remeshing engines provide no control on the final vertices coordinates and only limited control of their number or local density, generally determined by tolerance values. Above all, these methods force the use of a digital model as a starting point. As explained in "Methods", this makes the processing of curve and surface semi-landmarks complex and not intuitive when dealing with high morphological variations, like in the Theropod Dataset (Fig. 1). However, these procedures can prove perfectly suited for studies with relatively homogeneous sample morphologies as found in Gunz et al. (2005), or in the Shrew Dataset (Fig. 2). References and reviews on remeshing and non-rigid registration methods can be found in Alliez et al. (2005, 2008), Andresen et al. (2000), Andresen and Nielsen (2001).

On the contrary, our method allows one to design regular meshes from scratch with low-level mesh operations (vertex or edge insertion, translation). Hence, it provides complete control over the number, the coordinates and local density of the points composing the template. More importantly, it allows one to choose the level of geometrical complexity desired, which appears necessary to efficiently handle extremely opposed cases of morphological variation among a given sample. Finally, it is possible to achieve an anisotropic modelling adapted to the morphological features (Figs. 2 and 3). Hence, the template can easily be designed in order to be predivided into subregions of interest, that can be studied as separate modules in subsequent analyses.

As a result, we consider it is advisable to begin the study of any new structure with true landmarks exclusively. This can be a very helpful step in defining and fine-tuning the composition of the template before switching to more complex and time-demanding processes implied by using curve or surface semi-landmarks.

Acknowledgments

This article is a contribution of the "Plate-forme de Morphométrie" (MNHN, Paris) of CNRS UMS 2700 "Outils et Méthodes de la Systématique Intégrative", E. Pasquet dir. It benefited from the useful assistance and comments of Sibyle Moulin, Anne-Claire Fabre, Tharavy Douc and Céline Houssin, as well as from constructive discussions with Anick Abourachid, Vincent Debat, Noémie Bonneau and Gheylen Daghfous. We thank two anonymous reviewers for essential comments and criticisms, and Mickaël Coquerelle for kindly offering help and advices in using Edgewarp. The authors are also grateful to Brenda Chinnery-Allgeier for scanning the *Allosaurus* specimen

and Jack Horner and Pat Leiggi for facilitating access to the Museum of the Rockies for purposes of the scans. This research is funded by the 2008 SESAME grant from Région Île-de-France and contributions of CNRS UMR 7205 "Origine, Structure et Évolution de la Biodiversité", CNRS UMR 7209 "Archéozoologie, Archéobotanique : Sociétés, Pratiques et Environnements", CNRS UMR 7207 "Centre de Recherche sur la Paléobiodiversité et les Paléoenvironnements", CNRS UMR 7179 "Mécanismes adaptatifs : des organismes aux communautés". Extant specimens were scanned with support from MNHN ATM "Formes Possibles, Formes Réalisées", MNHN ATM "Plate-formes" and CNRS GDR 2474 "Morphométrie et Évolution des Formes".

References

Adams, D.C., Rohlf, F.J., 2000. Ecological character displacement in Plethodon: biomechanical differences found from a geometric morphometric study. PNAS 97 (8), 4106–4111.

Adams, D.C., Rohlf, F.J., Slice, D.E., 2004. Geometric morphometrics: ten years of progress following the "revolution". Ital. J. Zool. 71 (9), 5–16.

Alliez, P., De Verdière, C., Devilliers, O., Isenburg, M., 2005. Isotropic surface remeshing. Graphical Models 67 (3), 204–231.

Alliez, P., Ucelli, G., Gotsman, C., Attene, M., 2008. Recent advances in remeshing surfaces. In: De Floriani, L., Spagnuolo, M. (Eds.), Shape analysis and structuring, mathematics and visualization. Springer, Berlin, 296 p.

Andresen, P.R., Nielsen, M., 2001. Non-rigid registration by geometry-constrained diffusion. Med. Image Anal. 5, 81–88.

Andresen, P.R., Bookstein, F.L., Conradsen, K., Ersboll, B.K., Marsh, J.L., Kreiborg, S., 2000. Surface-bounded growth modeling applied to human mandibles. IEEE Trans. Med. Imaging 19 (11), 1053–1063.

Baylac, M., Friess, M., 2005. Fourier descriptors, Procrustes superimposition, and data dimensionality: an example of cranial shape analysis in modern human populations. In: Slice, D. (Ed.), Modern Morphometrics in Physical Anthropology. Kluwer Academic/Plenum Publishers, New York, pp. 145–165, 383 p.

Bookstein, F.L., 1991. Morphometric tools for landmark data: geometry and biology. Cambridge University Press, New York, 435 p.

Bookstein, F.L., 1996. Combining the tools of geometric morphometrics. In: Marcus, L.F., Corti, M., Loy, A., Naylor, G.J.P., Slice, D.E. (Eds.), Advances in morphometrics. Plenum Press, York, pp. 131–151, 587 p.

Bookstein, F.L., 1997. Landmark methods for forms without landmarks: morphometrics of group differences in outline shape. Med. Image Anal. 1 (3), 225–243.

Bookstein, F.L., 1998. A hundred years of morphometrics. Acta Zoologica Academiae Scientarium Hungaricae 44 (1–2), 7–59.

Bookstein, F.L., Green, W.D.K., 2002. Users Manual, EWSH3.19, http://brainmap.stat.washington.edu/edgewarp/.

Churchfield, S., 1990. Natural history of shrews. Christopher Helm, London, 178 p.

Darroch, J.N., Mosimann, J.E., 1985. Canonical and principal components of shape. Biometrika 72, 241–252.

Dryden, I.L., Mardia, K.V., 1998. Statistical shape analysis. John Wiley and Sons, New York, 347 p.

Ferson, S., Rohlf, F.J., Koehn, R.K., 1985. Measuring shape variation of two-dimensional outlines. Syst. Zool. 34, 59–68.

Gatesy, S.M., 1995. Functional evolution of the hind limb and tail from basal theropods to birds. In: Thomason, J.J. (Ed.), Functional morphology in vertebrate paleontology. Cambridge Univ. Press, Cambridge, pp. 219–234, 296 p.

Gunz, P., Mitteroecker, P., Bookstein, F.L., 2005. Semi-landmarks in three dimensions. In: Slice, D. (Ed.), Modern Morphometrics in Physical Anthropology. Kluwer Academic/Plenum Publishers, New York, 383 p.

Hertel, F., Campbell Jr., K.E., 2007. The antitrochanter of birds: form and function in balance. Auk 124 (3), 789–805.

Hutchinson, J.R., 2001. The evolution of pelvic osteology and soft tissues on the line to extant birds (Neornithes). Zool. J. Linn. Soc. 131, 123–168.

Hutchinson, J.R., 2004a. Biomechanical modeling and sensitivity analysis of bipedal running ability. I. Extant taxa. J. Morph. 262, 421–440.

Hutchinson, J.R., 2004b. Biomechanical modeling and sensitivity analysis of bipedal running ability. II. Extinct taxa. J. Morph. 262, 441–461.

Hutchinson, J.R., Gatesy, S.M., 2000. Adductors, abductors, and the evolution of archosaur locomotion. Paleobiology 26, 734–751.

Jardine, N., 1969. The observational and theoretical components of homology: a study based on the morphology of the dermal skull-roofs of rhipistidian fishes. Biol. J. Linn. Soc. 1, 327–349.

Klingenberg, C.P., 1996. Multivariate allometry. In: Marcus, L.F., Corti, M., Loy, A., Naylor, G.J.P., Slice, D.E. (Eds.), Advances in morphometrics. Plenum Press, New York, pp. 23–49.

Krzanowski, W.T., 1988. Principles of multivariate analysis: a user's perspective. Oxford University Press, New York, 608 p.

Kuhl, F.P., Giardina, C.R., 1982. Elliptical Fourier features of a closed contour. Comp. Graph. Imag. Proc. 18, 236–285.

Mardia, K.V., Bookstein, F.L., Moreton, I.J., 2000. Statistical assessment of bilateral symmetry of shapes. Biometrika 87 (2), 285–300.

McLeod, N., 1999. Generalizing and extending the eigenshape method of shape space visualization and analysis. Paleobiology 25 (1), 107–138.

Mitteroecker, P., Gunz, P., 2009. Advances in geometric morphometrics. Evol. Bio. 36, 235–247.

Monteiro, L.R., 1999. Multivariate regression models and geometric morphometrics: the search for causal factors in the analysis of shape. Syst. Biol. 48 (1), 192–199.

Mosimann, J.E., James, F.C., 1979. New statistical methods for allometry with application to Florida red-winged blackbirds. Evolution 33, 444–459.

Needham, A.E., 1950. The form transformation of the abdomen of the peacrab, *Pinnotheres pisum* Leach. Proc. Roy. Soc. London B 137, 115–136.

Rasskin-Gutman, D., Buscaglioni, A.D., 2001. Theoretical morphology of the Archosaurs (*Reptilia Diapsida*) Pelvic Girdle. Paleobiology 27 (1), 59–78.

Reilly, S.M., 2000. Locomotion in quail (*Coturnix japonica*): the kinematics of walking and increasing speed. J. Morphol. 243, 173–185.

Rohlf, F.J., 2000. On the use of shape spaces to compare morphometric methods. Hystrix 11 (1), 8–24.

Rohlf, F.J., Corti, M., 2000. Use of two-block partial least-squares to study covariation in shape. Syst. Biol. 49 (4), 740–753.

Rohlf, F.J., Marcus, L.F., 1993. A revolution in morphometrics. Trends Ecol. Evol. 8 (4), 129–132.

Rohlf, F.J., Slice, D.E., 1990. Extensions of the Procrustes method for the optimal superimposition of landmarks. System. Zool. 39, 40–59.

Rubenson, J., Lloyd, D.G., Besier, T.F., Heliams, D.B., Fournier, P.A., 2007. Running in ostriches (*Struthio camelus*): three-dimensional joint axes alignment and joint kinematics. J. Exp. Biol. 210, 2548–2562.

Slice, D.E., 2005. Modern morphometrics. In: Slice, D. (Ed.), Modern Morphometrics in Physical Anthropology. Kluwer Academic/Plenum Publishers, New York, 383 p.

Small, C.G., 1996. The statistical theory of shape. Springer-Verlag, New York, 227 p.

Wiley, D.F., Amenta, N., Alcantara, D.A., Ghosh, D., Kil, Y.J., Delson, E., Harcourt-Smith, W., Rohlf, F.J., St. John, K., Hamann, B., 2005. Evolutionary morphing, in: Proceedings of IEEE Visualization 2005 (VIS'05), 23–28 October 2005, Minneapolis, MN, USA.